

Probing Identity-Specific Motion Signatures: A Controlled Diagnostic Study

Yingtie Lei^{*1} Fangxun Liu^{*1} Baicheng Wu^{*1} Colin Lee¹ Ziheng Zhang¹ Junke Yang¹
 Zhiyuan Tao¹ Xuyan Huang¹ Shuheng Wang¹ William Koran¹ Kyle Park¹
 Elijah H. Buckwalter¹ Cheng-Hsuan Chiang¹ Tejas Naik¹ Daniel Yi¹ Wei-Lun Chao^{†1,2}

¹The Ohio State University ²Boston University

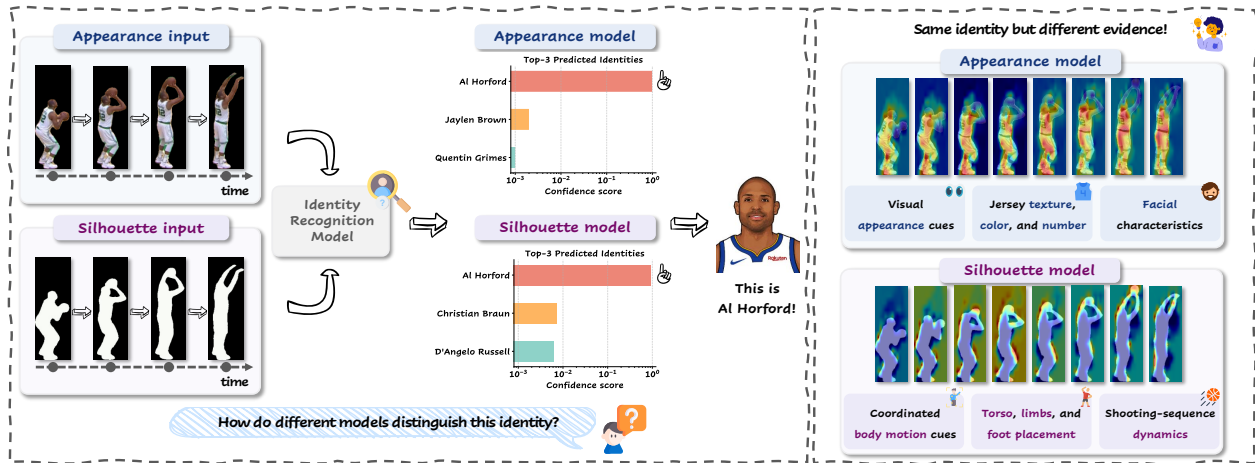


Figure 1. Overview of our diagnostic probe for identity-specific motion signatures. Given the same free-throw sequence, models can rely on appearance cues, such as jersey texture, color, number, and facial characteristics, or on appearance-suppressed silhouettes that preserve motion dynamics. By contrasting appearance and silhouette models, we examine *whether modern video models move beyond static visual shortcuts and capture human-interpretable motion patterns that serve as identity-specific signatures*.

Abstract

Identity recognition (e.g., person, animal re-identification) has traditionally relied heavily on static appearance cues. Yet motion—consistent, individual-specific dynamics—can provide a complementary and potentially more robust signature, especially when appearance is weak or variable. This raises a fundamental question: **when identity-specific motion cues are clearly present, to what extent do modern video models use them for recognition?** To investigate this question, we conduct a systematic diagnostic study and introduce **BALLER120**, a controlled benchmark of 120 professional basketball players performing free-throws. By focusing on the same multi-phase action across individuals, BALLER120 reduces action-level variation and identity-correlated acquisition biases, enabling fine-grained analysis of identity-specific kinematic patterns. We find that modern video models can predict identity accurately from RGB videos, but often rely on static appearance cues such

as faces and jersey regions, even when informative motion cues are available. Strikingly, when appearance is suppressed through silhouette-only or skeleton-only inputs, the same model architectures shift toward motion micro-patterns (e.g., foot placement and elbow bending). Despite containing less visual information, appearance-suppressed representations achieve competitive accuracy and stronger robustness to appearance shifts. Our qualitative analyses further show that appearance-suppressed models attend to distinctive motion patterns across individuals. Overall, our study demonstrates that identity-specific motion signatures are present, informative, and learnable, but modern video models may overlook them in favor of easier static shortcuts unless appearance cues are explicitly suppressed.

1. Introduction

Visual recognition has advanced rapidly, progressing from coarse category recognition to fine-grained subtype classification and individual identity recognition [1–4]. Mod-

^{*}Equal contributions.

[†]Corresponding author.

ern deep learning models now achieve strong performance across a wide range of recognition tasks [5–9]. Beyond enabling practical applications, this progress raises a deeper scientific opportunity: *accurate models may reveal visual or behavioral traits that are difficult for humans to explicitly characterize*. This possibility is especially intriguing for identity recognition, where the cues that distinguish one individual from another are often subtle and fine-grained.

One such cue is motion. Humans and animals exhibit consistent individual-specific dynamics that can persist across contexts [10, 11]. Unlike static appearance, which may be ambiguous, degraded, or altered over time, motion can reflect biomechanical habits that are harder to change or disguise. For example, observers can often recognize athletes from their pitching, shooting, or running styles even without a clear view of the face or jersey. This makes video-based identity recognition promising for uncovering subtle and previously unknown motion signatures.

However, before this promise can be realized, we must first ask a more basic diagnostic question: *do video models actually use motion patterns for identity recognition?* High recognition accuracy alone does not show that a model uses motion. It may instead rely on static cues, such as faces, clothing, or body patterns, or on incidental correlations introduced during data collection. In unconstrained video collections, identity may be correlated with nuisance factors such as action type, skill level, capture location, camera viewpoint, or environmental context. A model may thus recognize identities by exploiting dataset-specific shortcuts rather than learning how an individual moves.

This motivates a *controlled* setting in which identity-specific motion cues are clearly present and interpretable, while identity-correlated acquisition biases are reduced. We curate **BALLER120**, a controlled diagnostic dataset designed to probe motion signatures in identity recognition. BALLER120 contains over 4,500 short *free-throw* clips of 120 professional basketball players, collected across diverse games and broadcast camera viewpoints. Free-throws provide a useful testbed because they are structured, multi-phase actions shared across individuals: each sequence includes preparation, upward motion, ball release, and follow-through. Focusing on professional players further reduces coarse variation due to skill level, allowing us to study subtle but recognizable identity-specific differences in posture, timing, and body coordination. To further separate motion from static appearance, we provide frame-wise silhouette masks and body skeletons for each sequence, suppressing visual cues such as facial details, jersey numbers, and logos and encouraging models to rely more on *how players move*.

Using BALLER120, we evaluate whether modern video backbones actually rely on motion when repurposed for identity recognition. We study MViTv2 [12], VideoMAEV2 [13], and UniFormerV2 [14], originally devel-

oped for action recognition, under three input regimes: full-appearance, silhouette-only, and skeleton-only videos. For each regime, we fine-tune a separate model and evaluate it on held-out clips, allowing us to compare how recognition changes as static appearance cues are reduced.

As expected, models trained on full-appearance videos recognize players accurately, showing the strong transferability of modern pre-trained video backbones. More importantly, silhouette-only and skeleton-only models also achieve competitive accuracy, indicating that appearance-suppressed videos retain sufficient information for identity recognition. To examine what cues drive these predictions, we evaluate models under a split where each player’s static appearance distribution differs between training and testing. Full-appearance models degrade sharply under this shift, while appearance-suppressed models are more robust. Since full-appearance videos contain the same motion information available to silhouettes and skeletons, this contrast suggests that they do not lack motion cues; rather, they preferentially rely on static cues that fail to transfer across appearance changes. CAM-based saliency analysis [15] further supports this finding. When appearance is suppressed, models attend to motion micro-signatures that shift across body parts as the free-throw routine unfolds. These cues are stable across games and camera viewpoints for the same player, yet differ systematically across players performing the same action. In contrast, full-appearance models, despite having access to motion, concentrate largely on static regions such as faces and jerseys. These results suggest that motion cues are informative and identity-linked, but can be overshadowed by easier appearance shortcuts.

We further ask whether explicit appearance suppression is always necessary for learning motion signatures. To test whether this behavior is specific to identity recognition, we replace identity prediction with action discrimination, distinguishing three-pointers from free-throws using the same video backbones. In this setting, even full-appearance models attend to motion-relevant body regions rather than static appearance cues. This suggests a broader tendency: when optimized for accuracy, video models exploit the easiest predictive signal. For identity recognition, that signal is often static appearance; for action recognition, it is motion. Overall, our findings show that identity-specific motion signatures are present, learnable, and robust, but may be overlooked unless appearance cues are explicitly suppressed, pointing toward the need for video models that more reliably capture fine-grained individual dynamics.

Positioning. Existing identity recognition benchmarks, including re-identification and gait recognition [17–21], often emphasize recognition accuracy in unconstrained environments. Our objective is complementary: rather than pursuing generalization to unseen identities, actions, or domains, we ask what cues video models use when identity-specific

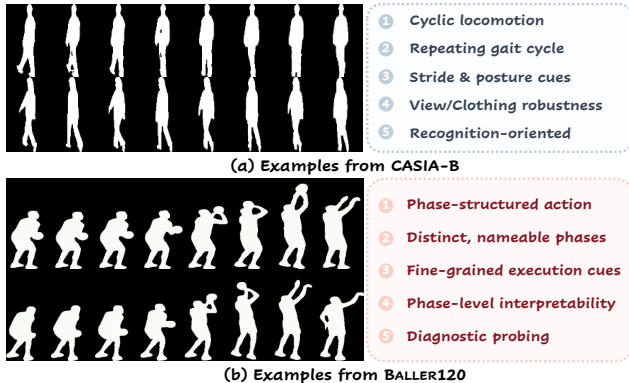


Figure 2. **Gait benchmarks vs. BALLER120.** Each row shows a different individual. BALLER120 is designed as a diagnostic probe: it focuses on free-throws, a multi-phase skilled action that naturally aligns execution across individuals, making it easier to visualize and verify the fine-grained identity-specific motion cues used by a model. In contrast, CASIA-B [16] focuses on identity recognition from cyclic walking motion, where inter-identity differences can be harder to inspect directly. BALLER120 therefore complements gait benchmarks as a diagnostic setting rather than a harder recognition benchmark.

motion cues are clearly present. We introduce a controlled benchmark and diagnostic protocol that reduce identity-correlated acquisition biases and separate static cues from motion-based identity cues. This controlled setting is a scientific design choice rather than a limitation.

Free-throws provide a suitable testbed: players perform the same structured, multi-phase action at a comparable professional standard; each identity has enough clips to reveal within-identity regularities; and the motion patterns can be directly inspected. While gait recognition has established motion as an important identity cue, walking is only one form of cyclic motion. Moreover, unconstrained datasets may inadvertently tie identity to viewpoint, clothing, scene, or capture conditions. BALLER120 complements prior benchmarks by focusing on skilled action, reducing incidental correlations, and exposing identity-specific motion signatures across interpretable phases (*i.e.*, set, rise, release, follow-through); see Fig. 2 for a comparison. To our knowledge, BALLER120 is the first controlled diagnostic dataset designed to make identity-specific motion signatures in skilled action discoverable and verifiable.

2. Related Work

Datasets for Identity Recognition. Existing datasets span three major settings. (1) **Person re-identification (Re-ID)** aims to match individuals across distinct observations. Image-based datasets, such as CUHK03 [22], Market-1501 [23], and MSMT17 [24], match cropped pedestrians across camera views. Video-based datasets, including iLIDS-VID [25] and MARS [26], use tracklets as the matching unit. To study stronger appearance variation,

PRCC [27], LTCC [28], and DeepChange [29] focus on clothing changes and long-term appearance shifts in image-based Re-ID, while CCVID [30] and MEVID [31] extend these settings to videos. (2) **Animal Re-ID** goes beyond human subjects and supports wildlife monitoring by recognizing individuals from visual biometric patterns, such as stripes, spots, fins, or facial-scale markings. WildlifeReID-10k [32], for example, provides a large-scale multi-species benchmark with over 10,000 individuals across diverse capture conditions. (3) **Gait recognition** studies identity from walking patterns, typically using short video clips, with representative datasets including CASIA-B [16], GREW [19], Gait3D [20], and CCPG [21]. We provide a detailed comparison between these datasets and BALLER120 in Table 1. **Biometrics for Identity Recognition.** Physiological biometrics provide stable identity cues [33–36], but often raise privacy concerns. Behavioral biometrics instead recognize individuals from how they move or act. Gait recognition shows walking patterns can carry identity-discriminative information across changes in viewpoint, clothing, and sensing condition [16, 19–21, 37, 38]. However, gait focuses on cyclic locomotion, a relatively regular form of motion. Richer actions contain more varied spatio-temporal structure, yet large-scale datasets such as Kinetics [39–41], Moments-in-Time [42], and Something-Something [43] focus on *what action is performed*, not *who performs it*. Whether fine-grained action dynamics can serve as identity-specific biometric cues remains underexplored.

3. Diagnostic Protocol Design

Overview. We study the question: *when identity-specific motion cues are clearly present, to what extent do modern video models use them for identity recognition?* As discussed in §1, high accuracy alone does not show that a model relies on motion: identity may correlate with appearance, action type, skill level, or data acquisition conditions. We therefore design BALLER120 as a *diagnostic probe* rather than a general-purpose benchmark. Our goal is to reduce dataset-specific biases and separate cues into two groups: *execution-independent* cues, such as a player’s face or jersey, which identify the player regardless of movement; and *execution-dependent* cues, which reflect how the action is performed. This design allows us to suppress the former and inspect the latter. BALLER120 implements this idea through four criteria: (i) controlling coarse action-level variation, (ii) suppressing execution-independent appearance and anatomy, (iii) exposing execution-dependent evidence through complementary input regimes, and (iv) supporting human-interpretable, phase-level attribution.

Controlling Action and Context. We focus on a single standardized action: the basketball free-throw, performed by all identities at a comparable professional level. Holding the action constant reduces coarse action- and scene-

level differences common in unconstrained videos, while restricting to professional players narrows skill-level variation. This makes inter-person differences concentrate more on how each player executes the same routine. The shared multiple phases (set, rise, release, and follow-through) also make the setting diagnosable, allowing evidence to be compared at corresponding moments.

Suppressing Execution-independent Appearance and Anatomy. We reduce two types of cues that can identify a player regardless of motion. Static appearance, such as face, jersey, and texture, is removed through silhouette videos derived from frame-wise masks. Fixed anatomy, such as absolute scale and height, is reduced by spatially normalizing each sequence to a common scale; see §4. The remaining signal thus depends more on how the body moves than on static appearance or body size. We also consider skeletons from off-the-shelf pose estimators, which further abstract away appearance and body shape.

Exposing Execution-dependent Evidence. We examine the cues that remain after suppression: how each player executes the same routine. Some cues appear within a single phase, such as the set posture, release pose, or follow-through configuration. These are not fixed anatomy, since they depend on how the player performs the action. Other cues unfold over time, such as transitions between phases. Since no single representation captures all of these signals, we study complementary regimes: silhouettes preserve the dense body envelope, while skeletons preserve sparse joint positions and motion.

Supporting Human-interpretable Attribution. We use the structure of the free-throw as a natural vocabulary for inspection. When attribution highlights a body region, it can be linked to an observable execution pattern within a specific phase. We therefore treat attribution as diagnostic support rather than standalone proof, and ask whether a model’s evidence is stable within identity, distinct across identities, and aligned with interpretable phases.

4. The BALLER120 Dataset

Dataset Construction. Following the diagnostic protocol in §3, we curate BALLER120 from official NBA broadcast replays, focusing on free-throw sequences. The pipeline is shown in Fig. 3. Each clip is manually trimmed from the end of dribbling to shot release, and verified to ensure the target player remains visible and trackable throughout. Free-throw scenarios also naturally reduce player occlusion, yielding more reliable segmentation masks.

Localizing and Tracking Target Players. Given a trimmed clip, we feed the first frame into Grounding DINO [44], prompted with text queries to localize all visible players. The target player is manually identified, and their bounding box is passed as a spatial prompt to SAM2 [45], which propagates frame-wise segmentation masks across

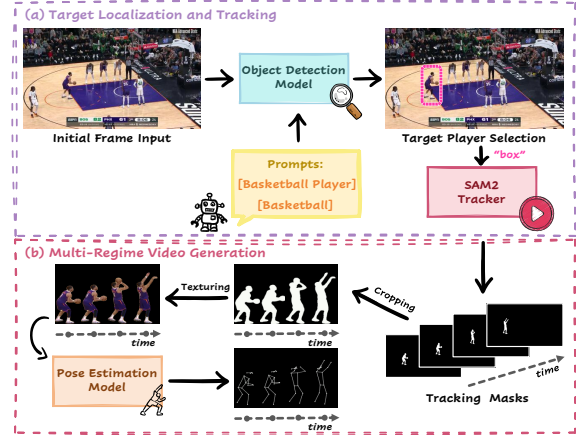


Figure 3. Data pipeline. (a) We localize all players in the first frame using Grounding DINO [44] prompted by text queries, manually select the target, and pass the box to SAM2 [45] to propagate frame-wise masks. (b) From the tracked masks, we generate three input regimes: appearance, silhouette, and skeleton.

the entire sequence. To ensure temporal consistency, the basketball is included in the player mask prior to shot release and excluded afterward, so that the ball’s trajectory is not encoded as part of the player’s motion.

Generating Multi-Regime Videos. Using the frame-wise masks, we crop each clip around the player with a single union bounding box over all frames, and resize the crop to a common scale while preserving aspect ratio. This removes per-frame jitter and absolute size while keeping the action’s spatial range intact, reducing reliance on camera position and body scale, which are execution-independent. Within the cropped region, we derive three input regimes. *Appearance videos* preserve the visual content inside the mask while removing background context. *Silhouette videos* retain only the binary mask, suppressing face, jersey, and texture while keeping how the body is configured and moves through the routine. *Skeleton videos* render sparse body keypoints estimated from the appearance frames using RTMPose [46], discarding the dense body envelope while retaining joint configuration and temporal progression.

Dataset Statistics. As illustrated in Fig. 4, BALLER120 comprises 4,583 free-throw sequences across 120 professional NBA players from all 30 teams, averaging roughly 38 clips per identity, collected across games, viewpoints, and jersey appearances. Each clip captures a complete free-throw averaging 1.71 seconds (~ 2.18 hours total), and is provided in appearance, silhouette, and skeleton regimes.

Dataset Comparison. Table 1 situates BALLER120 among representative Re-ID and gait datasets, which are typically curated for recognition accuracy in unconstrained or view-varying settings. In contrast, BALLER120 is built for diagnosis: it asks which cues a model uses, not only how accurately it recognizes. This goal is reflected in the action design. Re-ID datasets leave actions unconstrained, and gait



Figure 4. Per-identity clip distribution across the 120 NBA players in BALLER120. Colors denote NBA teams; numbers and bar lengths indicate clip counts per player.

Table 1. **Comparison of BALLER120 with representative identity-recognition datasets.** BALLER120 complements Re-ID and gait benchmarks by focusing on a multi-phase skilled action with paired appearance and appearance-suppressed video regimes, enabling diagnostic analysis of identity-relevant execution cues.

Dataset	Scale		Data Type	Action Protocol	App. Suppression	Explain. Support
	#IDs	#Box/#Seq				
<i>Person Re-identification</i>						
CUHK03 [22]	1,360	13,164	Image	None	⊗	⊗
Market-1501 [23]	1,501	32,668	Image	None	⊗	⊗
MSMT17 [24]	4,101	126,441	Image	None	⊗	⊗
PRCC [27]	221	33,698	Image	None	⊗	⊗
LTCC [28]	152	17,138	Image	None	⊗	⊗
DeepChange [29]	1,121	178,407	Image	None	⊗	⊗
iLIDS-VID [25]	300	600	Video	None	⊗	⊗
MARS [26]	1,261	20,715	Video	None	⊗	⊗
CCVID [30]	226	2,856	Video	None	⊗	⊗
MEVID [31]	158	8,092	Video	None	⊗	⊗
<i>Gait Recognition</i>						
CASIA-B [16]	124	13,640	Video	Cyclic gait	✓	⊗
GREW [19]	26,345	128,671	Video	Cyclic gait	✓	⊗
Gait3D [20]	4,000	25,309	Video	Cyclic gait	✓	⊗
CCPG [21]	200	16,566	Video	Cyclic gait	✓	⊗
BALLER120	120	4,583	Video	Multi-phase skilled	✓	✓

datasets focus on cyclic locomotion, whereas BALLER120 fixes a multi-phase skilled action shared across identities, making inter-person variation more attributable to individual execution than to action type or scene. BALLER120 also pairs each sequence with appearance-suppressed silhouette and skeleton regimes, whose cues can be inspected phase by phase to support interpretable diagnosis. These choices explain its scale: with 120 identities, roughly 38 clips per identity, and dense annotations, BALLER120 is smaller than large-scale Re-ID benchmarks but comparable to gait datasets such as CASIA-B and CCPG. BALLER120 therefore complements existing benchmarks by filling a gap they were not designed to address.

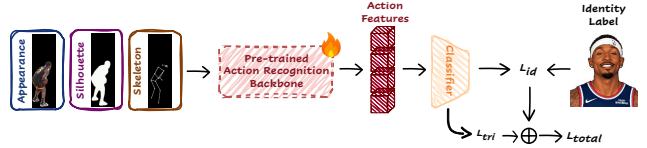


Figure 5. **Identity probing with action-recognition backbones.** Each video, in one of three input regimes (appearance, silhouette, or skeleton), is passed through a fully fine-tuned (🔥) backbone, whose embedding is optimized with an identity classification loss \mathcal{L}_{id} and a triplet loss \mathcal{L}_{tri} .

5. Repurposing Action-Recognition Backbones for Identity Probing

Action recognition (AR) and identity recognition pursue different objectives: AR classifies *what action occurs*, whereas identity recognition determines *who an individual is*, often from static appearance. Since all our clips depict the same free-throw, coarse action-category differences cannot explain identity prediction, letting us ask a sharper question: with the action fixed, can video backbones adapt to identity-discriminative evidence in *how* it is executed?

We use pre-trained AR backbones as a diagnostic basis. These models are not built for identity recognition, but their representations encode motion dynamics and body configuration. We repurpose them by replacing the action classification head with a linear identity classifier and fully fine-tuning the backbone (e.g., UniFormerV2 [14] pre-trained on Kinetics-400 [39]). This does not assume the learned evidence is purely motion-based; rather, it lets us compare how identity evidence changes as appearance is available or suppressed. As shown in Fig. 5, the backbone maps each video to an embedding \mathbf{e} optimized for identity, applied identically across appearance, silhouette, and skeleton regimes.

We train with two complementary objectives. The *classification path* feeds \mathbf{e} into the identity classifier to produce logits \mathbf{z} over N identities, with cross-entropy and label smoothing ($\epsilon = 0.1$):

$$\mathcal{L}_{id} = - \sum_{k=1}^N q(k) \log p(k), \quad (1)$$

where $p(k) = \text{softmax}(\mathbf{z})_k$ and $q(k) = (1 - \epsilon)\delta_{k,y} + \epsilon/N$ for true label y . The *metric-learning path* applies a batch-hard triplet loss to \mathbf{e} , pulling same-identity samples closer than different-identity ones by a margin $m = 0.3$:

$$\mathcal{L}_{tri} = \sum_{i=1}^B \left[\max_{\mathbf{e}_p \in \mathcal{P}_i} d(\mathbf{e}_i, \mathbf{e}_p) - \min_{\mathbf{e}_n \in \mathcal{N}_i} d(\mathbf{e}_i, \mathbf{e}_n) + m \right]_+, \quad (2)$$

where B is the batch size, $[\cdot]_+ = \max(0, \cdot)$, $d(\cdot, \cdot)$ is the Euclidean distance, and $\mathcal{P}_i, \mathcal{N}_i$ denote the positive and negative samples for anchor \mathbf{e}_i within the batch. The final objective is

$$\mathcal{L}_{total} = \mathcal{L}_{id} + \mathcal{L}_{tri}. \quad (3)$$

Table 2. Closed-set performance under the **standard** split. For each backbone, the gap is computed relative to the appearance-input model; gait methods are evaluated as standalone baselines.

Model	Input	Classification			Retrieval		
		Top-1 (%)	Top-3 (%)	Top-5 (%)	mAP (%)	R-1 (%)	R-5 (%)
MViTv2 [12]	App.	98.60	99.30	99.51	98.46	98.82	98.82
	Sil.	98.39 $\downarrow 0.21$	99.37 $\uparrow 0.07$	99.51 -0.00	98.31 $\downarrow 0.15$	98.67 $\downarrow 0.15$	98.82 -0.00
	Skel.♣	97.84 $\downarrow 0.76$	99.16 $\downarrow 0.14$	99.30 $\downarrow 0.21$	97.07 $\downarrow 1.39$	97.64 $\downarrow 1.18$	97.79 $\downarrow 1.03$
VideoMAEV2 [13]	App.	98.04	98.95	99.16	97.93	98.53	98.53
	Sil.	95.46 $\downarrow 2.58$	98.67 $\downarrow 0.28$	99.09 $\downarrow 0.07$	95.58 $\downarrow 2.35$	97.64 $\downarrow 0.89$	98.08 $\downarrow 0.45$
UniFormerV2 [14]	App.	97.49	99.02	99.30	89.35	97.20	98.97
	Sil.	95.67 $\downarrow 1.82$	98.25 $\downarrow 0.77$	98.95 $\downarrow 0.35$	85.95 $\downarrow 3.40$	95.13 $\downarrow 2.07$	97.49 $\downarrow 1.48$
<i>Gait Recognition Methods</i>							
BigGait [38]	App.	99.51	99.79	99.86	98.27	99.41	99.41
DeepGaitV2 [47]	Sil.	99.72	99.79	99.79	98.72	99.26	99.41

♣ We only report the MViTv2 results for the skeleton input (see §6.2).

Table 3. Closed-set performance under the **appearance-disjoint** split. Gaps are relative to the same backbone’s appearance input.

Model	Input	Classification			Retrieval		
		Top-1 (%)	Top-3 (%)	Top-5 (%)	mAP (%)	R-1 (%)	R-5 (%)
MViTv2 [12]	App.	5.31	13.62	19.24	57.63	84.90	92.26
	Sil.	89.07 $\uparrow 83.76$	95.66 $\uparrow 82.04$	96.95 $\uparrow 77.71$	86.12 $\uparrow 28.49$	92.64 $\uparrow 7.74$	95.94 $\uparrow 3.68$
	Skel.	93.95 $\uparrow 88.64$	97.68 $\uparrow 84.06$	98.47 $\uparrow 79.23$	92.08 $\uparrow 34.45$	96.32 $\uparrow 11.42$	97.97 $\uparrow 5.71$
VideoMAEV2 [13]	App.	1.34	6.54	10.20	59.61	89.72	94.04
	Sil.	84.42 $\uparrow 83.08$	92.91 $\uparrow 86.37$	95.42 $\uparrow 85.22$	78.94 $\uparrow 19.33$	90.86 $\uparrow 1.14$	94.92 $\uparrow 0.88$
UniFormerV2 [14]	App.	22.85	43.80	57.06	54.70	85.66	93.27
	Sil.	88.82 $\uparrow 65.97$	94.56 $\uparrow 50.76$	95.60 $\uparrow 38.54$	74.83 $\uparrow 20.13$	92.89 $\uparrow 7.23$	97.46 $\uparrow 4.19$

6. Experiment and Analysis

6.1. Experimental Setup

Model Architecture. We adapt three pre-trained action-recognition backbones for identity recognition: MViTv2 [12], VideoMAEV2 [13], and UniFormerV2 [14]. MViTv2 and UniFormerV2 are initialized with Kinetics-400 weights, while VideoMAEV2 uses Kinetics-710 weights. VideoMAEV2 and UniFormerV2 use ViT-B/16 encoders, whereas MViTv2 uses the small variant. We further compare against two dedicated motion-based identity recognition baselines, BigGait [38] and DeepGaitV2 [47].

Metric. We report both the accuracy of the identity classifier and the retrieval performance of the learned feature embeddings (e.g., mAP and Rank- k : whether the top- k retrieved clips contain at least one correct identity).

Data Split. We use two strategies. The standard split divides each identity’s clips into train/test at 7:3, with test clips further split into query/gallery at 5:5. The appearance-disjoint split instead partitions clips by jersey appearance, so each identity’s train and test clips have disjoint appearance, using the same query/gallery protocol.

Implementation Details. All models are trained for 100 epochs using AdamW [48] with cosine annealing. Input frames are resized to 224×224 , and each clip is sampled to 16 frames. We use random horizontal flipping, color jittering, random erasing, and a random identity sampler during training, and uniform frame sampling during testing. We evaluate three input regimes, following the pipeline described in §4: appearance, silhouette, and skeleton.

6.2. Main Results

Can General Video Backbones Recognize Identity?

General video backbones recognize players reliably once repurposed for identity, even though identity recognition is not their original design goal. As shown in Table 2, under the standard split, where each identity’s clips are divided randomly so that appearance distributions overlap between training and testing, full-appearance input drives all three action-recognition backbones to near-perfect accuracy.

A deeper question is what remains once appearance is removed. The silhouette and skeleton regimes strip away face, jersey, and texture, keeping how the body is configured and how it moves. Both stay competitive with full appearance, dropping only marginally. Identity-specific motion is therefore not merely present in these clips; it is readily learnable even when appearance is suppressed. The dedicated gait models reach comparable near-ceiling accuracy under the same protocol, suggesting that the identity signal in free-throw execution is not specific to a single architecture.

Interestingly, the two appearance-suppressed regimes are not equivalent. Silhouettes are more compatible with standard video backbones, likely because they remain video-like while preserving dense body shape and fine-grained motion cues that sparse skeletons may discard. They perform consistently well across architectures. Skeletons transfer less reliably; only MViTv2 remains robust in this regime, so we report skeleton results only for MViTv2.

What Survives When Appearance Shifts? Models trained under different regimes may rely on different identity cues. Under the standard split, where both appearance and motion can transfer, it remains unclear which cues drive recognition. To separate them, we evaluate the appearance-disjoint split. As shown in Table 3, when each identity’s training and test clips differ in jersey appearance, full-appearance models degrade sharply, while appearance-suppressed models remain robust and outperform appearance models across the board. Since full-appearance videos contain the same mo-

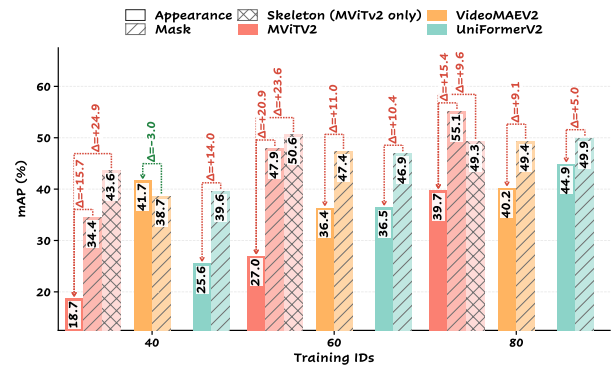


Figure 6. Open-set performance under the appearance-disjoint setting. Appearance-suppressed regimes (striped, diamond-hatched bars) stay mostly ahead across training scales, indicating that motion-based representations transfer to unseen identities.

Table 4. Impact of contour degradation (\mathcal{B}) on silhouette-based (Sil.) models. Despite the degradation, all models retain strong performance, confirming that recognition relies on motion dynamics rather than fine-grained boundary details.

Model	Input	Classification			Retrieval		
		Top-1 (%)	Top-3 (%)	Top-5 (%)	mAP (%)	R-1 (%)	R-5 (%)
MViTv2 [12]	Sil.	98.39	99.37	99.51	98.31	98.67	98.82
	Sil.+ \mathcal{B}	97.00 $\downarrow 1.39$	99.16 $\downarrow 0.21$	99.37 $\downarrow 0.14$	95.11 $\downarrow 3.20$	97.49 $\downarrow 1.18$	98.23 $\downarrow 0.59$
VideoMAEV2 [13]	Sil.	95.46	98.67	99.09	95.58	97.64	98.08
	Sil.+ \mathcal{B}	92.04 $\downarrow 3.42$	96.37 $\downarrow 2.30$	97.49 $\downarrow 1.60$	88.38 $\downarrow 7.20$	92.77 $\downarrow 4.87$	95.28 $\downarrow 2.80$
UniFormerV2 [14]	Sil.	95.67	98.25	98.95	85.95	95.13	97.49
	Sil.+ \mathcal{B}	94.76 $\downarrow 0.91$	97.56 $\downarrow 0.69$	98.18 $\downarrow 0.77$	83.29 $\downarrow 2.66$	94.10 $\downarrow 1.03$	97.64 $\downarrow 0.15$



Figure 7. Original vs. contour-degraded silhouettes: fine boundaries are blurred while body motion is retained.

tion information available to silhouettes and skeletons, this gap indicates that appearance models do not fail because motion cues are absent; rather, they rely on appearance cues that do not transfer once jerseys change. By contrast, the cues recovered under suppression are not generic shortcuts, but individual-specific motion patterns.

We next test whether these motion cues extend to unseen identities, *i.e.*, the open-set setting. Under the appearance-disjoint split, we hold out 40 test identities and gradually increase the number of training identities. As shown in Fig. 6, appearance-suppressed regimes perform the best mostly, with gains persisting as training scale grows. With appearance shortcuts shifted and identities unseen, recognition must rely more on subtle motion cues that appearance usually overshadows, indicating that these cues are genuine and transferable rather than tied to the training identities.

Sanity Check: Shape or Execution? Silhouettes suppress face, jersey, and texture, but their contours still trace a body outline, so recognition could rest on fixed shape rather than on how the action is executed. We test this by degrading contour fidelity while leaving the temporal structure intact. As illustrated in Fig. 7, each binary mask is downsampled and reconstructed by bicubic interpolation, blurring fine boundaries while preserving how the body moves; the shape cue is weakened, the execution cue is kept. As shown in Table 4, recognition is largely unaffected: across all three backbones, the drop is marginal, and accuracy stays high even when boundaries are coarse. If the models were reading identity from precise contours, this degradation should substantially reduce performance. The observed stability suggests instead that recognition does not hinge on fixed shape, but on execution-dependent evidence.

6.3. Main Analysis

To reveal these identity-specific *motion signatures* in a verifiable, interpretable form, we use CAM-based saliency [15], examining whether the evidence is tied to each player’s execution, stable across views, and distinct across players.

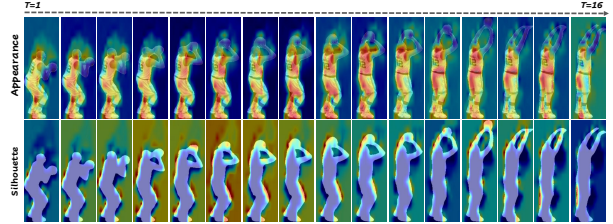


Figure 8. Saliency maps for the same player (Al Horford). The appearance model attends to jersey and face regions, whereas the silhouette model shifts with the unfolding free-throw.

Different Regimes Attend to Different Cues. As shown in Fig. 8, the two regimes focus on different evidence for the same player. The appearance model focuses on the jersey and face, holding attention on static regions across the whole sequence. The silhouette model instead shifts its focus as the action unfolds: attention starts on the back and legs as the shot begins, shifts to the thighs and arms during the rise, and concentrates on the arms at release. This frame-by-frame alignment with the shooting motion indicates that the silhouette model tracks how the action is executed rather than what the player looks like. Beyond visual inspection, we quantify saliency by grouping pixels into four regions—head, torso, arms, and legs—and aggregating attention within each region per frame (Fig. 9). For appearance input, regional saliency stays flat across the sequence, dominated by the jersey-bearing torso and legs. For silhouette input, the curves rise and fall with the phases of the shot: arm and leg saliency grows as the limbs elevate, while the torso stays low throughout. The attention is therefore not a static spatial bias but a temporally organized response that follows the execution itself.

Signature Holds Across Viewpoints. Motion signatures should persist regardless of viewpoint. In Fig. 10, we compare saliency for the same player across clips captured from different broadcast angles. Despite the change in viewpoint, the silhouette model traverses the same body regions in the same temporal order, reproducing the player’s execution

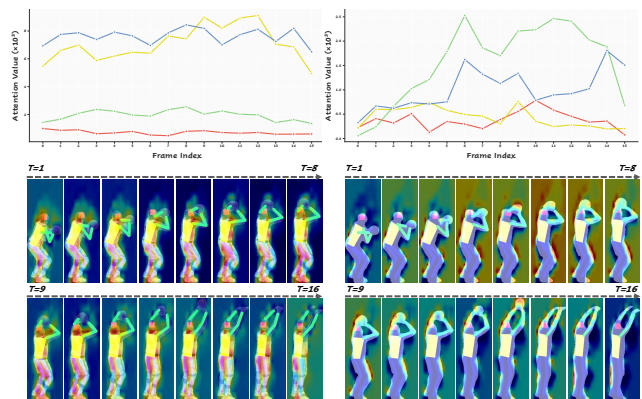


Figure 9. Pose-based quantification of attention dynamics. Saliency is aggregated per frame over four regions—Head, Torso, Arms, Legs. Appearance saliency is flat over time; silhouette saliency tracks the shot phases.

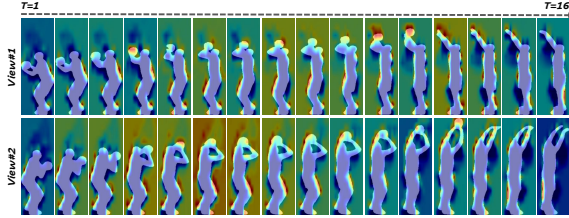


Figure 10. Saliency maps of the same player across different camera viewpoints. The silhouette model follows the same body regions in the same temporal order, showing that the motion evidence is stable within an identity.

pattern rather than a view-dependent artifact. The evidence the model relies on is thus stable within an identity.

Each Player Has a Distinctive Signature. In Fig. 11, two players performing the identical action draw distinct attention. For the fast, explosive shooter, the model concentrates on rapid arm elevation and elbow trajectory in the early frames, whereas for the more deliberate shooter, it attends to foot placement and arm configuration throughout, including the post-release follow-through. Applied to the same action, the model surfaces different evidence for each identity—confirming that what it captures reflects individual execution style, not a generic free-throw template.

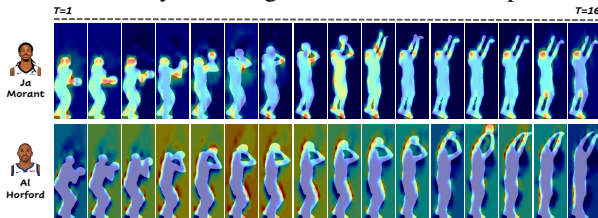


Figure 11. Saliency maps for Ja Morant and Al Horford performing free-throws. The model attends to different body regions per player, showing that the evidence is distinct across identities.

6.4. Further Exploration and Investigation

Is Appearance Suppression Needed to Use Motion Cues? Silhouette models reliably encode identity-specific motion, whereas full-appearance models often do not. This raises a question: do video models use motion only when appearance is suppressed? To test this, we curate three-pointer clips for 109 players and fine-tune a full-appearance backbone for binary action recognition: three-pointers vs. free-throws. As shown in Fig. 12, the task changes what the model attends to. For action recognition, saliency follows the shooting execution—arm elevation, release trajectory, and torso lift—even without appearance suppression. Yet these cues are shared across players: they capture *what* action is performed, not *who* performs it. For identity recognition, the same model family shifts toward static appearance, suggesting that appearance provides an easier identity signal that overshadows subtler kinematic cues. We call this *task-induced appearance bias*: models favor visual shortcuts when they predict the training objective. Only by

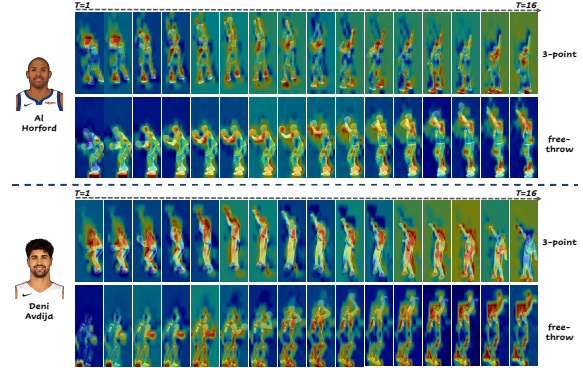


Figure 12. Saliency maps under action recognition between three-pointers and free-throws. Identity-specific motions are overshadowed by shared, action-defining patterns common across players.

Table 5. Probing whether static frames carry motion signatures, across four input regimes: App., Sil., Sil.+ β , and Skel.

Input	Frame(s)	App.		Sil.		Sil.+ β		Skel.	
		Acc (%)	Conf	Acc (%)	Conf	Acc (%)	Conf	Acc (%)	Conf
Image (DINOv3 [9])	First	93.09 \pm 4.08	0.63 \pm 0.27	77.23 \pm 18.16	0.49 \pm 0.29	72.63 \pm 19.16	0.47 \pm 0.28	45.60 \pm 19.74	0.36 \pm 0.24
	Multiple	96.65 \pm 6.27	0.85 \pm 0.17	90.43 \pm 11.19	0.69 \pm 0.24	91.97 \pm 10.67	0.71 \pm 0.24	93.92 \pm 9.03	0.65 \pm 0.24
Video (MVTV2 [12])	Multiple	98.60 \pm 4.46	0.99 \pm 0.05	98.39 \pm 4.86	0.98 \pm 0.07	97.00 \pm 5.86	0.96 \pm 0.12	97.84 \pm 5.31	0.98 \pm 0.08
		98.04 \pm 5.31	1.00 \pm 0.03	95.46 \pm 7.67	0.98 \pm 0.08	92.04 \pm 12.01	0.96 \pm 0.13	—	—
Video (UniFormerV2 [14])	Multiple	97.49 \pm 5.43	0.83 \pm 0.22	95.67 \pm 6.88	0.82 \pm 0.22	94.76 \pm 7.80	0.79 \pm 0.24	—	—

fixing the action and suppressing appearance are models pushed toward genuine identity-specific motion. This further supports our controlled design: unconstrained actions introduce semantic variation, while intact appearance draws models toward shortcuts and away from the execution cues needed to study motion-based identity recognition.

Do Motion Signatures Reside in Static Frames? As discussed in §3, some identity cues may appear within individual phases, such as the set posture and release pose. We ask whether such within-phase poses are sufficient to identify a player without continuous video. To test this, we use an image backbone, DINOv3 [9], with the same classification head and training protocol as before. The model is trained either on a single starting frame or on the same frames used by the video models, treated as independent still images. Table 5 shows that static poses are informative: a single frame already supports identity recognition, and using all frames recovers much of the gap to video models. However, image models remain less confident than video models at comparable accuracy, with the key difference being whether frames are processed in temporal order. Static poses thus capture part of the motion signature, but temporal relationships across phases provide more robust identity evidence. Continuous motion, rather than isolated snapshots, remains the stronger cue.

7. Conclusion

We introduce BALLER120, a controlled diagnostic probe, to study a fundamental question: when identity-specific motion is clearly present, do modern video models rely on it for recognition? When appearance is suppressed, video models under silhouette and skeleton regimes remain competitive in

recognition; attribution further indicates that their evidence is tied to how each player executes the action. Yet without suppression, models still default to appearance shortcuts. These findings show that identity-specific motion signatures are present, learnable, and verifiable, but easily overlooked, pointing toward video models that more reliably capture fine-grained individual dynamics.

Acknowledgments

This research is supported in part by grants from the National Science Foundation (Imageomics Institute: NSF OAC-2118240). We are grateful for the generous support from the Ohio Supercomputer Center.

References

- [1] Jia Deng, Wei Dong, Richard Socher, Li-Jia Li, Kai Li, and Li Fei-Fei. Imagenet: A large-scale hierarchical image database. In *2009 IEEE conference on computer vision and pattern recognition*, pages 248–255. Ieee, 2009. 1
- [2] Alex Krizhevsky, Ilya Sutskever, and Geoffrey E Hinton. Imagenet classification with deep convolutional neural networks. *Advances in neural information processing systems*, 25, 2012.
- [3] Mang Ye, Jianbing Shen, Gaojie Lin, Tao Xiang, Ling Shao, and Steven CH Hoi. Deep learning for person re-identification: A survey and outlook. *IEEE transactions on pattern analysis and machine intelligence*, 44(6):2872–2893, 2021.
- [4] Xiu-Shen Wei, Yi-Zhe Song, Oisín Mac Aodha, Jianxin Wu, Yuxin Peng, Jinhui Tang, Jian Yang, and Serge Belongie. Fine-grained image analysis with deep learning: A survey. *IEEE transactions on pattern analysis and machine intelligence*, 44(12):8927–8948, 2021. 1
- [5] Alec Radford, Jong Wook Kim, Chris Hallacy, Aditya Ramesh, Gabriel Goh, Sandhini Agarwal, Girish Sastry, Amanda Askell, Pamela Mishkin, Jack Clark, et al. Learning transferable visual models from natural language supervision. In *International conference on machine learning*, pages 8748–8763. PmLR, 2021. 2
- [6] Zhuang Liu, Hanzi Mao, Chao-Yuan Wu, Christoph Feichtenhofer, Trevor Darrell, and Saining Xie. A convnet for the 2020s. In *Proceedings of the IEEE/CVF conference on computer vision and pattern recognition*, pages 11976–11986, 2022.
- [7] Xiaohua Zhai, Basil Mustafa, Alexander Kolesnikov, and Lucas Beyer. Sigmoid loss for language image pre-training. In *Proceedings of the IEEE/CVF international conference on computer vision*, pages 11975–11986, 2023.
- [8] Yi Wang, Xinhao Li, Ziang Yan, Yinan He, Jiashuo Yu, Xiangyu Zeng, Chenting Wang, Changlian Ma, Haiyan Huang, Jianfei Gao, et al. Internvideo2.5: Empowering video mllms with long and rich context modeling. *arXiv preprint arXiv:2501.12386*, 2025.
- [9] Oriane Siméoni, Huy V Vo, Maximilian Seitzer, Federico Baldassarre, Maxime Oquab, Cijo Jose, Vasil Khalidov, Marc Szafraniec, Seungeun Yi, Michaël Ramamonjisoa, et al. Dinov3. *arXiv preprint arXiv:2508.10104*, 2025. 2, 8
- [10] Claudio Filipi Gonçalves dos Santos, Diego De Souza Oliveira, Leandro A. Passos, Rafael Gonçalves Pires, Daniel Felipe Silva Santos, Lucas Pascotti Valem, Thierry P. Moreira, Marcos Cleison S. Santana, Mateus Roder, Jo Paulo Papa, et al. Gait recognition based on deep learning: A survey. *ACM Computing Surveys (CSUR)*, 55(2):1–34, 2022. 2
- [11] Chuanfu Shen, Shiqi Yu, Jilong Wang, George Q Huang, and Liang Wang. A comprehensive survey on deep gait recognition: Algorithms, datasets, and challenges. *IEEE Transactions on Biometrics, Behavior, and Identity Science*, 7(2): 270–292, 2024. 2
- [12] Yanghao Li, Chao-Yuan Wu, Haoqi Fan, Karttikeya Mangalam, Bo Xiong, Jitendra Malik, and Christoph Feichtenhofer. Mvitv2: Improved multiscale vision transformers for classification and detection. In *Proceedings of the IEEE/CVF conference on computer vision and pattern recognition*, pages 4804–4814, 2022. 2, 6, 7, 8
- [13] Limin Wang, Bingkun Huang, Zhiyu Zhao, Zhan Tong, Yinan He, Yi Wang, Yali Wang, and Yu Qiao. Videomae v2: Scaling video masked autoencoders with dual masking. In *Proceedings of the IEEE/CVF conference on computer vision and pattern recognition*, pages 14549–14560, 2023. 2, 6, 7, 8, 5
- [14] Kunchang Li, Yali Wang, Yinan He, Yizhuo Li, Yi Wang, Limin Wang, and Yu Qiao. Uniformerv2: Unlocking the potential of image vits for video understanding. In *Proceedings of the IEEE/CVF International Conference on Computer Vision*, pages 1632–1643, 2023. 2, 5, 6, 7, 8
- [15] Bolei Zhou, Aditya Khosla, Agata Lapedriza, Aude Oliva, and Antonio Torralba. Learning deep features for discriminative localization. In *Proceedings of the IEEE conference on computer vision and pattern recognition*, pages 2921–2929, 2016. 2, 7
- [16] Shiqi Yu, Daoliang Tan, and Tieniu Tan. A framework for evaluating the effect of view angle, clothing and carrying condition on gait recognition. In *18th international conference on pattern recognition (ICPR’06)*, pages 441–444. IEEE, 2006. 3, 5
- [17] Liang Zheng, Hengheng Zhang, Shaoyan Sun, Manmohan Chandraker, Yi Yang, and Qi Tian. Person re-identification in the wild. In *Proceedings of the IEEE conference on computer vision and pattern recognition*, pages 1367–1376, 2017. 2
- [18] Stefan Schneider, Graham W Taylor, Stefan Linquist, and Stefan C Kremer. Past, present and future approaches using computer vision for animal re-identification from camera trap data. *Methods in Ecology and Evolution*, 10(4):461–470, 2019.
- [19] Zheng Zhu, Xianda Guo, Tian Yang, Junjie Huang, Jiankang Deng, Guan Huang, Dalong Du, Jiwen Lu, and Jie Zhou. Gait recognition in the wild: A benchmark. In *Proceedings of the IEEE/CVF international conference on computer vision*, pages 14789–14799, 2021. 3, 5
- [20] Jinkai Zheng, Xinchun Liu, Wu Liu, Lingxiao He, Chenggang Yan, and Tao Mei. Gait recognition in the wild with

- dense 3d representations and a benchmark. In *Proceedings of the IEEE/CVF conference on computer vision and pattern recognition*, pages 20228–20237, 2022. 3, 5
- [21] Weijia Li, Saihui Hou, Chunjie Zhang, Chunshui Cao, Xu Liu, Yongzhen Huang, and Yao Zhao. An in-depth exploration of person re-identification and gait recognition in cloth-changing conditions. In *Proceedings of the IEEE/CVF Conference on Computer Vision and Pattern Recognition*, pages 13824–13833, 2023. 2, 3, 5
- [22] Wei Li, Rui Zhao, Tong Xiao, and Xiaogang Wang. Deepreid: Deep filter pairing neural network for person re-identification. In *Proceedings of the IEEE conference on computer vision and pattern recognition*, pages 152–159, 2014. 3, 5
- [23] Liang Zheng, Liyue Shen, Lu Tian, Shengjin Wang, Jingdong Wang, and Qi Tian. Scalable person re-identification: A benchmark. In *Proceedings of the IEEE international conference on computer vision*, pages 1116–1124, 2015. 3, 5
- [24] Longhui Wei, Shiliang Zhang, Wen Gao, and Qi Tian. Person transfer gan to bridge domain gap for person re-identification. In *Proceedings of the IEEE conference on computer vision and pattern recognition*, pages 79–88, 2018. 3, 5
- [25] Taiqing Wang, Shaogang Gong, Xiatian Zhu, and Shengjin Wang. Person re-identification by video ranking. In *European conference on computer vision*, pages 688–703. Springer, 2014. 3, 5
- [26] Liang Zheng, Zhi Bie, Yifan Sun, Jingdong Wang, Chi Su, Shengjin Wang, and Qi Tian. Mars: A video benchmark for large-scale person re-identification. In *European conference on computer vision*, pages 868–884. Springer, 2016. 3, 5
- [27] Qize Yang, Ancong Wu, and Wei-Shi Zheng. Person re-identification by contour sketch under moderate clothing change. *IEEE transactions on pattern analysis and machine intelligence*, 43(6):2029–2046, 2019. 3, 5
- [28] Xuelin Qian, Wenxuan Wang, Li Zhang, Fangrui Zhu, Yanwei Fu, Tao Xiang, Yu-Gang Jiang, and Xiangyang Xue. Long-term cloth-changing person re-identification. In *Proceedings of the Asian conference on computer vision*, 2020. 3, 5
- [29] Peng Xu and Xiatian Zhu. Deepchange: A long-term person re-identification benchmark with clothes change. In *Proceedings of the IEEE/CVF International Conference on Computer Vision*, pages 11196–11205, 2023. 3, 5
- [30] Xinqian Gu, Hong Chang, Bingpeng Ma, Shutao Bai, Shiguang Shan, and Xilin Chen. Clothes-changing person re-identification with rgb modality only. In *Proceedings of the IEEE/CVF conference on computer vision and pattern recognition*, pages 1060–1069, 2022. 3, 5
- [31] Daniel Davila, Dawei Du, Bryon Lewis, Christopher Funk, Joseph Van Pelt, Roderic Collins, Kellie Corona, Matt Brown, Scott McCloskey, Anthony Hoogs, and Brian Clipp. Mevid: Multi-view extended videos with identities for video person re-identification. In *Proceedings of the IEEE/CVF Winter Conference on Applications of Computer Vision (WACV)*, pages 1634–1643, 2023. 3, 5
- [32] Lukas Adam, Vojtech Cermák, Kostas Papafitsoros, and Lukas Pícek. Wildlifereid-10k: Wildlife re-identification dataset with 10k individual animals. In *Proceedings of the IEEE/CVF Conference on Computer Vision and Pattern Recognition*, pages 2124–2134, 2025. 3
- [33] Andrew J Calder and Andrew W Young. Understanding the recognition of facial identity and facial expression. *Nature Reviews Neuroscience*, 6(8):641–651, 2005. 3
- [34] John Daugman. How iris recognition works. In *The essential guide to image processing*, pages 715–739. Elsevier, 2009.
- [35] Sharath Pankanti, Salil Prabhakar, and Anil K Jain. On the individuality of fingerprints. *IEEE Transactions on pattern analysis and machine intelligence*, 24(8):1010–1025, 2002.
- [36] Chin-Chuan Han, Hsu-Liang Cheng, Chih-Lung Lin, and Kuo-Chin Fan. Personal authentication using palm-print features. *Pattern recognition*, 36(2):371–381, 2003. 3
- [37] Ming Wang, Xianda Guo, Beibei Lin, Tian Yang, Zheng Zhu, Lincheng Li, Shunli Zhang, and Xin Yu. Dygait: Exploiting dynamic representations for high-performance gait recognition. In *Proceedings of the IEEE/CVF international conference on computer vision*, pages 13424–13433, 2023. 3
- [38] Dingqiang Ye, Chao Fan, Jingzhe Ma, Xiaoming Liu, and Shiqi Yu. Biggait: Learning gait representation you want by large vision models. In *Proceedings of the IEEE/CVF conference on computer vision and pattern recognition*, pages 200–210, 2024. 3, 6
- [39] Will Kay, Joao Carreira, Karen Simonyan, Brian Zhang, Chloe Hillier, Sudheendra Vijayanarasimhan, Fabio Viola, Tim Green, Trevor Back, Paul Natsev, et al. The kinetics human action video dataset. *arXiv preprint arXiv:1705.06950*, 2017. 3, 5
- [40] Joao Carreira, Eric Noland, Andras Banki-Horvath, Chloe Hillier, and Andrew Zisserman. A short note about kinetics-600. *arXiv preprint arXiv:1808.01340*, 2018.
- [41] Joao Carreira, Eric Noland, Chloe Hillier, and Andrew Zisserman. A short note on the kinetics-700 human action dataset. *arXiv preprint arXiv:1907.06987*, 2019. 3
- [42] Mathew Monfort, Alex Andonian, Bolei Zhou, Kandan Ramakrishnan, Sarah Adel Bargal, Tom Yan, Lisa Brown, Quanfu Fan, Dan Gutfreund, Carl Vondrick, et al. Moments in time dataset: one million videos for event understanding. *IEEE transactions on pattern analysis and machine intelligence*, 42(2):502–508, 2019. 3
- [43] Raghav Goyal, Samira Ebrahimi Kahou, Vincent Michalski, Joanna Materzynska, Susanne Westphal, Heuna Kim, Valentin Haenel, Ingo Fruend, Peter Yianilos, Moritz Mueller-Freitag, et al. The “something something” video database for learning and evaluating visual common sense. In *Proceedings of the IEEE international conference on computer vision*, pages 5842–5850, 2017. 3
- [44] Shilong Liu, Zhaoyang Zeng, Tianhe Ren, Feng Li, Hao Zhang, Jie Yang, Qing Jiang, Chunyuan Li, Jianwei Yang, Hang Su, et al. Grounding dino: Marrying dino with grounded pre-training for open-set object detection. In *European conference on computer vision*, pages 38–55. Springer, 2024. 4
- [45] Nikhila Ravi, Valentin Gabeur, Yuan-Ting Hu, Ronghang Hu, Chaitanya Ryali, Tengyu Ma, Haitham Khedr, Roman Rädle, Chloe Rolland, Laura Gustafson, Eric Mintun, Junt-

- ing Pan, Kalyan Vasudev Alwala, Nicolas Carion, Chao-Yuan Wu, Ross Girshick, Piotr Dollár, and Christoph Feichtenhofer. Sam 2: Segment anything in images and videos. *arXiv preprint arXiv:2408.00714*, 2024. 4
- [46] Tao Jiang, Peng Lu, Li Zhang, Ningsheng Ma, Rui Han, Chengqi Lyu, Yining Li, and Kai Chen. Rtmpose: Real-time multi-person pose estimation based on mmpose. *arXiv preprint arXiv:2303.07399*, 2023. 4
- [47] Chao Fan, Saihui Hou, Yongzhen Huang, and Shiqi Yu. Exploring deep models for practical gait recognition. *arXiv preprint arXiv:2303.03301*, 2023. 6
- [48] Ilya Loshchilov and Frank Hutter. Decoupled weight decay regularization. In *ICLR*, 2019. 6
- [49] Marco Tulio Ribeiro, Sameer Singh, and Carlos Guestrin. ” why should i trust you?” explaining the predictions of any classifier. In *Proceedings of the 22nd ACM SIGKDD international conference on knowledge discovery and data mining*, pages 1135–1144, 2016. 2
- [50] Scott M Lundberg and Su-In Lee. A unified approach to interpreting model predictions. *Advances in neural information processing systems*, 30, 2017. 2
- [51] David Baehrens, Timon Schroeter, Stefan Harmeling, Motoaki Kawanabe, Katja Hansen, and Klaus-Robert Müller. How to explain individual classification decisions. *The Journal of Machine Learning Research*, 11:1803–1831, 2010. 2
- [52] Ramprasaath R Selvaraju, Michael Cogswell, Abhishek Das, Ramakrishna Vedantam, Devi Parikh, and Dhruv Batra. Grad-cam: Visual explanations from deep networks via gradient-based localization. In *Proceedings of the IEEE international conference on computer vision*, pages 618–626, 2017. 2
- [53] Aditya Chattopadhyay, Anirban Sarkar, Prantik Howlader, and Vineeth N Balasubramanian. Grad-cam++: Generalized gradient-based visual explanations for deep convolutional networks. In *2018 IEEE winter conference on applications of computer vision (WACV)*, pages 839–847. IEEE, 2018.
- [54] Haofan Wang, Zifan Wang, Mengnan Du, Fan Yang, Zijian Zhang, Sirui Ding, Piotr Mardziel, and Xia Hu. Score-cam: Score-weighted visual explanations for convolutional neural networks. In *Proceedings of the IEEE/CVF conference on computer vision and pattern recognition workshops*, pages 24–25, 2020. 2
- [55] Ziheng Zhang, Jianyang Gu, Arpita Chowdhury, Zheda Mai, David Carlyn, Tanya Berger-Wolf, Yu Su, and Wei-Lun Chao. Finer-cam: Spotting the difference reveals finer details for visual explanation. In *Proceedings of the Computer Vision and Pattern Recognition Conference*, pages 9611–9620, 2025. 2

Probing Identity-Specific Motion Signatures: A Controlled Diagnostic Study

Supplementary Material

This supplementary material provides additional implementation details and analyses that support the diagnostic findings in the main paper. It is organized as follows:

- Appendix A reports the backbone configurations and training hyperparameters used in our experiments.
- Appendix B clarifies how saliency maps are used as diagnostic evidence and defines our interpretation criteria.
- Appendix C provides additional skeleton-input results and discusses why skeleton compatibility differs across backbones.
- Appendix D visualizes skeleton-based saliency patterns to inspect identity-specific execution evidence.
- Appendix E reports complementary open-set results under the standard split.
- Appendix F examines whether identity evidence comes from static frames or ordered temporal progression.
- Appendix G provides representation evidence by comparing retrieval neighborhoods and embedding spaces across regimes.
- Appendix H provides qualitative and quantitative evidence for stable and distinctive execution cues.
- Appendix I compares saliency patterns across backbones to show architecture-dependent evidence.

A. Additional Training Details

A.1. Backbone Configurations

For all three video backbones, we largely inherit the configurations from the corresponding pre-trained action recognition models, modifying only a few hyperparameters that significantly influence the fine-tuning performance (see Ta-

Table A1. Configuration of MViTv2, compared with the original configuration. Hyperparameter names follow the original configuration file. † denotes a value modified from the original setting.

Parameter	Ours	Original
BACKBONE	MViTv2-S	MViTv2-S
EMBED_DIM	96	96
DEPTH	16	16
NUM_HEADS	1	1
MLP_RATIO	4.0	4.0
PATCH_KERNEL	(3, 7, 7)	(3, 7, 7)
PATCH_STRIDE	(2, 4, 4)	(2, 4, 4)
PATCH_PADDING	(1, 3, 3)	(1, 3, 3)
DIM_MUL	{1, 3, 14} × 2	{1, 3, 14} × 2
HEAD_MUL	{1, 3, 14} × 2	{1, 3, 14} × 2
POOL_Q_STRIDE	(1, 2, 2) at {1, 3, 14}	(1, 2, 2) at {1, 3, 14}
POOL_KV_STRIDE_ADAPTIVE	[1, 8, 8]	[1, 8, 8]
POOL_KVQ_KERNEL	[3, 3, 3]	[3, 3, 3]
CLS_EMBED_ON	True	True
DROPPATH_RATE	0.2	0.2
DROPOUT_RATE	0.0	0.0

Table A2. Configuration of VideoMAEv2, compared with the original configuration. Hyperparameter names follow the original configuration file. † denotes a value modified from the original setting.

Parameter	Ours	Original
BACKBONE	vit_base_patch16_224	vit_base_patch16_224
embed_dim	768	768
depth	12	12
num_heads	12	12
mlp_ratio	4.0	4.0
patch_size	16	16
tubelet_size	2	2
use_mean_pooling	True	True
cos_attn	False	False
drop_path_rate†	0.0	0.1
drop_rate†	0.2	0.0
attn_drop_rate	0.0	0.0
head_drop_rate	0.0	0.0

Table A3. Configuration of UniFormerV2, compared with the original configuration. Hyperparameter names follow the original configuration file. † denotes a value modified from the original setting.

Parameter	Ours	Original
BACKBONE	uniformerv2_b16	uniformerv2_b16
N_DIM	768	768
N_HEAD	12	12
N_LAYERS	4	4
MLP_FACTOR	4.0	4.0
RETURN_LIST	[8, 9, 10, 11]	[8, 9, 10, 11]
TEMPORAL_DOWNSAMPLE	False	False
BACKBONE_DROP_PATH_RATE	0.0	0.0
DROP_PATH_RATE	0.0	0.0
MLP_DROPOUT	[0.5, 0.5, 0.5, 0.5]	[0.5, 0.5, 0.5, 0.5]
CLS_DROPOUT	0.5	0.5
NO_LMHRA†	False	True
DOUBLE_LMHRA	True	True
DW_REDUCTION	1.5	1.5

bles A1 to A3). We adjust these hyperparameters using the closed-set standard split in §6.1, and then fix them for all other experiments. Namely, we treat the test set of the standard split as the validation set. The test sets of other experiments are never used for hyperparameter selection.

For ease of comparison, the hyperparameters in Tables A1 to A3 follow the descriptions used in the original configuration files/model definitions, and hyperparameters that differ from the original setting are marked with †.

We refer the reader to the official repositories for the original configurations that our settings are based on:

- MViTv2:  [facebookresearch/SlowFast](https://github.com/facebookresearch/SlowFast)
- VideoMAEv2:  [OpenGVLab/VideoMAEv2](https://github.com/OpenGVLab/VideoMAEv2)
- UniFormerV2:  [OpenGVLab/UniFormerV2](https://github.com/OpenGVLab/UniFormerV2)

Table A4. Training hyperparameters for fine-tuning the three backbones.

Parameter	MViTv2	UniFormerV2	VideoMAEv2
Optimizer	AdamW	AdamW	AdamW
Weight decay	0.05	0.05	0.05
LR schedule	Cosine	Cosine	Cosine
Base (peak) LR	1e-4	1e-4	1e-4
Final LR	1e-6	1e-6	1e-6
Total epochs	100	100	100
Batch size	16	16	8

A.2. Training Hyperparameters

We summarize the optimization settings used to fine-tune the three backbones in Table A4. Some of these details were already stated in §6.1 of the main paper, and are repeated here for completeness. All three backbones are fully fine-tuned with AdamW (weight decay 0.05), a peak learning rate of 1e-4, a cosine annealing learning-rate schedule decaying to a final learning rate of 1e-6, and a total of 100 epochs. The only difference is the batch size: VideoMAEv2 uses a batch size of 8 due to its higher memory footprint, while MViTv2 and UniFormerV2 use 16.

B. Attribution Methods and Diagnostic Scope

B.1. Background

Saliency-based attribution estimates which spatial or spatio-temporal regions of an input contribute to a trained model’s prediction. Existing approaches include perturbation- or optimization-based explanations [49, 50], gradient-based saliency [51], and class activation mapping (CAM) methods [15, 52–55]. CAM-based methods are commonly used in visual recognition because they project class-discriminative evidence from intermediate feature maps back to the input domain. Grad-CAM [52] uses class-specific gradients as activation weights, while Score-CAM [54] estimates these weights through forward activation scores. For fine-grained recognition, Finer-CAM [55] further suppresses activations shared across visually similar classes to highlight more class-specific evidence.

B.2. Role In Diagnostic Protocol

In BALLER120, saliency maps are used as diagnostic support rather than standalone proof of identity-specific motion, following the diagnostic protocol described in §3. This distinction is important because appearance-suppressed inputs, especially silhouettes, still preserve body outline, phase-specific pose, and coarse configuration. We therefore do not interpret a highlighted silhouette region as direct evidence of “pure motion.” Instead, we use saliency to inspect how the evidence used by a trained identity classifier changes across the input regimes defined in §4: ap-

Table C1. Skeleton-input performance under the **standard** split across three video backbones. The MViTv2 result is included from Table 2 for direct comparison.

Model	Input	Classification			Retrieval		
		Top-1 (%)	Top-3 (%)	Top-5 (%)	mAP (%)	R-1 (%)	R-5 (%)
MViTv2 [12]	Skel.	97.84	99.16	99.30	97.07	97.64	97.79
VideoMAEv2 [13]	Skel.	25.07	44.13	53.49	11.96	24.78	44.99
UniFormerV2 [14]	Skel.	87.92	95.53	97.00	55.38	80.53	93.22

pearance, silhouette, and skeleton. Full-appearance models reveal whether the classifier relies on static visual shortcuts such as face, jersey texture, color, or number. Silhouette and skeleton models reveal whether the same architectures shift toward execution-dependent evidence, such as foot placement, elbow bend, torso configuration, limb coordination, or transitions across free-throw phases.

B.3. Interpretation Criteria

Consistent with the analysis protocol in §6.3, we treat an attributed region as candidate identity-specific execution evidence only when it satisfies three criteria: (i) it is stable across clips, games, and viewpoints for the same player; (ii) it differs across players performing the same free-throw phase; and (iii) it aligns with an observable component of the free-throw routine, such as set posture, rise, release, or follow-through. This phase-level reading is enabled by the controlled structure of BALLER120. Accordingly, our saliency analysis is intended to localize candidate motion micro-signatures, while the overall claim is supported by the broader diagnostic design rather than by attribution alone.

C. Backbone Sensitivity to Skeleton Input

To complement the MViTv2 skeleton results discussed in §6.2, we additionally report the standard-split skeleton performance of VideoMAEv2 and UniFormerV2 in Table C1. These results show that compatibility with skeleton input is strongly backbone-dependent.

C.1. Backbone-dependent Skeleton Compatibility

Table C1 indicates that skeleton input is not equally effective across video backbones. MViTv2 remains highly robust under skeleton input, consistent with the observation in §6.2. UniFormerV2 also retains strong classification accuracy, although its retrieval performance is substantially weaker than that of MViTv2. In contrast, VideoMAEv2 degrades sharply across both classification and retrieval metrics. These results suggest that skeleton compatibility depends not only on the input regime itself, but also on how each backbone aggregates identity-relevant evidence from sparse spatio-temporal signals.

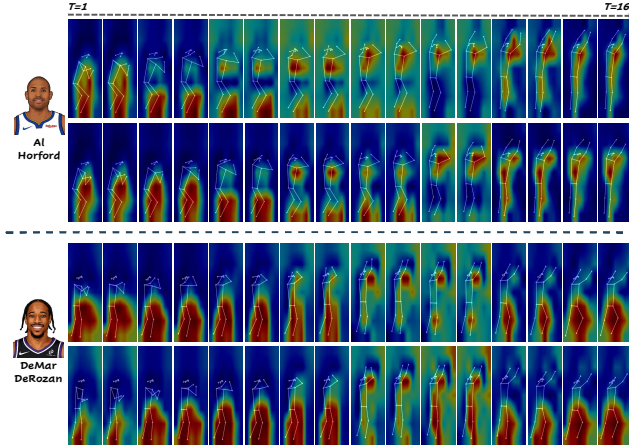


Figure D1. Skeleton saliency maps across players and clips. For the same player, saliency patterns remain broadly consistent across clips, indicating within-identity stability. Across players, the highlighted regions and temporal progression differ, suggesting identity-specific execution evidence. The maps also show a relatively global response over the skeleton sequence, consistent with the stronger MViTv2 skeleton performance reported in §C.

C.2. Interpretation from Saliency Patterns

A plausible interpretation is that different backbones aggregate identity evidence over the body at different spatial scales. This matters for skeleton input because skeletons preserve only sparse keypoints and their temporal progression, while removing the dense body envelope available in silhouettes. As a result, backbones that rely on broad, distributed body-level evidence may remain more compatible with skeletons, whereas backbones that depend more on localized regional evidence may be more sensitive to this sparsification.

As further illustrated in the backbone-level saliency comparison in §I, especially the left half of Fig. II, MViTv2 exhibits a more spatially distributed response over the player body. Its saliency covers lower-body, torso, and upper-body regions as the free-throw progresses. UniFormerV2 shows a more region-focused pattern, with stronger emphasis on selected body parts and phase-specific configurations. VideoMAEV2 appears the most localized, concentrating saliency on smaller regions rather than broadly aggregating evidence across the full body. The skeleton results in Table C1 broadly follow this ordering: MViTv2, which shows the most globally distributed saliency pattern, is also the most robust to skeleton input, whereas VideoMAEV2, which shows the most localized pattern, suffers the largest degradation.

This difference is consistent with the input-regime design in §4. Silhouettes suppress face, jersey, and texture, but still preserve a dense body outline and rich spatial configuration. Skeletons further abstract the signal into sparse joints, which can weaken some execution-dependent cues

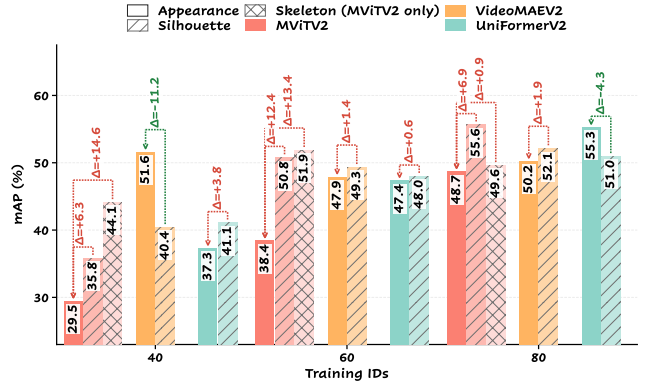


Figure E1. Open-set performance under the standard split. Appearance-suppressed regimes remain mostly ahead across training scales, showing that the trend observed under the appearance-disjoint setting also holds under a relatively easier protocol.

discussed in §3, including phase-specific body configuration, relative limb placement, torso alignment, and localized coordination patterns. Under this view, skeletonization does not remove all identity evidence, but it changes which forms of evidence remain accessible to each architecture.

This interpretation also supports the observation in §6.2 that silhouettes are generally more compatible with standard video backbones than skeletons. Silhouettes retain a denser representation of how the body is configured and moves through the routine, whereas skeletons provide a more compact and sparse abstraction. We therefore treat the saliency correspondence as a hypothesis consistent with the observed trends, not as independent causal evidence.

D. Skeleton Saliency Analysis

To further inspect the skeleton-input regime, we visualize CAM-based saliency maps for the MViTv2 skeleton model. This analysis complements the quantitative results in §C and follows the diagnostic criteria in §B.3: the attributed evidence should be stable within an identity, distinct across identities, and aligned with the free-throw execution.

As shown in Fig. D1, the skeleton model produces consistent saliency patterns for the same player across different clips. For Al Horford, the highlighted evidence follows a similar temporal progression across examples, with attention broadly distributed over the lower body and torso in early frames and shifting toward the upper body near release. For DeMar DeRozan, the model follows a different progression, emphasizing a distinct pattern of lower-body, torso, and upper-body evidence across the sequence. These differences indicate that the model is not simply responding to a generic skeleton template shared by all players; rather, it highlights player-specific execution patterns within the same structured action.

This visualization is also consistent with the backbone-level observation in §C.2. In particular, the saliency maps

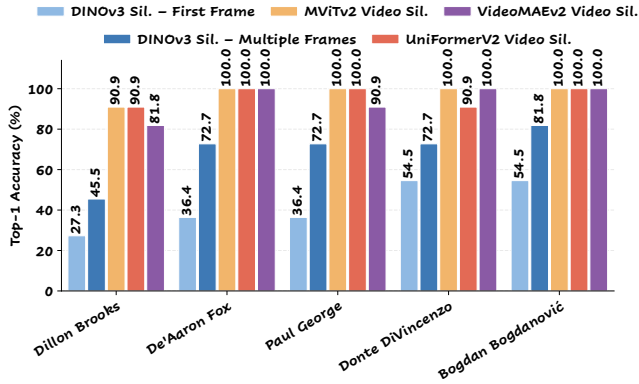


Figure F1. Per-identity static-frame analysis for silhouette inputs. Multiple frames improve over a single frame, while video models further exploit temporal execution cues.

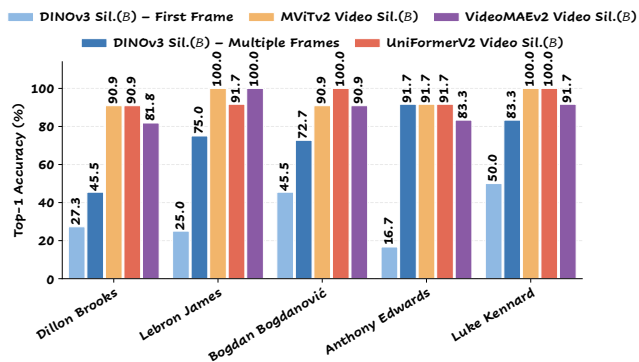


Figure F2. Per-identity static-frame analysis for contour-degraded silhouettes. Video models overall remain strong after contour degradation, supporting the role of temporal execution cues beyond static boundary information.

show a relatively global response over the skeleton sequence, rather than a narrowly localized focus on a single joint or region. Such distributed evidence may help explain why MViTv2 remains compatible with skeleton input: even after the dense body envelope is removed, the model can still aggregate identity-relevant cues across multiple body regions and phases. We therefore treat these maps as qualitative support for skeleton-based execution evidence, while maintaining the diagnostic scope discussed in §B.3.

E. Standard Open-set Results

In §6.2, we evaluate open-set recognition under the appearance-disjoint split, where training and test clips differ in jersey appearance. This protocol is intentionally strict: it reduces the usefulness of static appearance and tests whether appearance-suppressed representations transfer to unseen identities. Here, we add a complementary open-set evaluation under the standard split, where the held-out identities are still unseen but the train/test appearance distributions are not explicitly separated by jersey appearance.

As shown in Fig. E1, the overall trend remains consistent

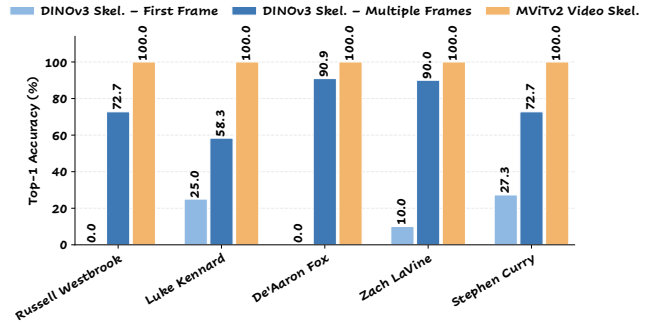


Figure F3. Per-identity static-frame analysis for skeleton inputs. Video modeling provides stronger identity evidence than isolated or independently processed static skeleton frames.

with the appearance-disjoint open-set results in §6.2. Although the standard split is less challenging and therefore yields smaller gains, appearance-suppressed regimes still outperform appearance in most settings. Silhouettes remain consistently competitive across backbones, and the MViTv2 skeleton results also stay strong when available. This supports the observation in §6.2 that identity-relevant execution cues are not limited to the appearance-disjoint protocol. These results should be read as complementary evidence rather than a replacement for the appearance-disjoint evaluation. The appearance-disjoint split remains the stricter test of robustness to appearance shifts, while the standard split shows that the same preference for appearance-suppressed representations largely persists even when the evaluation protocol is relatively easier.

F. Static Evidence and Temporal Ordering

§6.4 asks whether identity-specific motion signatures can be recovered from static frames, or whether ordered video provides additional evidence. We complement that analysis with two controlled probes. The first compares frame-based image representations with ordered video representations under appearance-suppressed regimes, testing how much identity evidence is already present in isolated or independently processed phases. The second disrupts temporal order by shuffling frames within each video, testing whether video models rely on the ordered progression of the free-throw routine rather than only on the unordered set of body configurations. Together, these analyses clarify the role of temporal structure: static poses provide partial identity evidence, but ordered execution across phases remains a stronger cue for motion-based identity recognition.

F.1. Frame-based vs. Video-based Recognition

The results in §6.4 show that static frames contain partial identity evidence, but ordered video provides stronger recognition. Here, we further inspect this gap at the identity level. Rather than showing randomly selected players, we focus on identities for which video modeling provides the

Table F1. Impact of temporal shuffling (\mathcal{S}) on VideoMAEV2 and UniFormerV2. Shuffling preserves the frames but removes their temporal order; the larger degradation for silhouette inputs indicates reliance on ordered execution dynamics.

Model	Input	Classification			Retrieval		
		Top-1 (%)	Top-3 (%)	Top-5 (%)	mAP (%)	R-1 (%)	R-5 (%)
VideoMAEV2 [13]	App.	98.04	98.95	99.16	97.93	98.53	98.53
	App.+ \mathcal{S}	96.93 \downarrow 1.11	98.74 \downarrow 0.21	99.09 \downarrow 0.07	96.10 \downarrow 1.83	97.33 \downarrow 1.20	97.88 \downarrow 0.65
	Sil.	95.46	98.67	99.09	95.58	97.64	98.08
	Sil.+ \mathcal{S}	43.78 \downarrow 51.68	60.68 \downarrow 37.99	69.13 \downarrow 29.96	31.83 \downarrow 63.75	55.27 \downarrow 42.37	76.19 \downarrow 21.89
UniFormerV2 [14]	App.	97.49	99.02	99.30	89.35	97.20	98.97
	App.+ \mathcal{S}	93.85 \downarrow 3.64	97.63 \downarrow 1.39	98.32 \downarrow 0.98	73.60 \downarrow 15.75	87.85 \downarrow 9.35	96.12 \downarrow 2.85
	Sil.	95.67	98.25	98.95	85.95	95.13	97.49
	Sil.+ \mathcal{S}	80.80 \downarrow 14.87	91.06 \downarrow 7.19	94.20 \downarrow 4.75	53.14 \downarrow 32.81	77.42 \downarrow 17.71	89.88 \downarrow 7.61

clearest benefit over frame-based recognition. This allows us to visualize cases where isolated or independently processed poses are insufficient, but ordered execution across the free-throw sequence remains discriminative.

Displayed identities are selected by comparing the average Top-1 accuracy of image-based DINOv3 representations across the first-frame and multiple-frame settings with the average Top-1 accuracy of the available video models. For each appearance-suppressed regime, we show the five identities with the largest improvement from frame-based to video-based recognition. For skeleton input, only MVITv2 is included as the available video model.

As shown in Figs. F1 to F3, static frames can already support identity recognition in some cases, especially when multiple phases are observed. This is consistent with the discussion in §3: some execution-dependent cues appear within individual phases, such as set posture, release pose, or follow-through configuration. However, video-based models remain stronger for the selected identities, indicating that these cues are not fully captured by isolated static configurations. Instead, identity evidence is distributed across the free-throw sequence, and ordered temporal relationships between phases provide additional discriminative information.

F.2. Temporal Shuffling

The frame-based analysis tests whether static phase information is sufficient. We next test whether temporal order itself matters by training and evaluating VideoMAEV2 and UniFormerV2 under the standard closed-set split after randomly permuting all frames within each clip. This preserves the same visual observations while disrupting the ordered progression of the free-throw routine.

As shown in Table F1, temporal shuffling affects appearance and silhouette models differently. Appearance models degrade only moderately, suggesting that they can still rely on static visual evidence. In contrast, silhouette models suffer substantially larger drops, especially for VideoMAEV2. Since silhouette inputs suppress face, jersey, and texture, this degradation indicates that the models are not merely using an unordered collection of body configurations; they also rely on the temporal ordering of execution cues. This

complements the frame-based analysis and further supports the conclusion in §6.4: static poses contain partial identity evidence, but ordered motion provides a more robust basis for probing identity-specific motion signatures.

G. Representation Evidence Across Regimes

The analyses in Secs. 6.2 to 6.4 show that appearance and appearance-suppressed models achieve recognition through different evidence: appearance models remain vulnerable to appearance shifts, whereas silhouette models preserve stronger robustness and attend to phase-aligned execution cues. Here, we provide a complementary representation-level view using UniFormerV2 as a representative backbone. Instead of asking where the model attends, we ask how the learned feature space organizes clips under different input regimes. We use nearest-neighbor retrieval and embedding visualization to inspect whether appearance and silhouette inputs induce different identity neighborhoods.

G.1. Nearest-neighbor Retrieval

We first compare retrieval neighborhoods under full-appearance and silhouette input. For each query clip, we retrieve the Top-5 nearest gallery clips from the learned embedding space. For silhouette retrieval, we display the corresponding full-appearance videos of the retrieved clips only for visual inspection; retrieval itself is performed using silhouette features.

As shown in Fig. G1, appearance-based retrieval often returns gallery clips with similar visual appearance, such as jersey color or texture, even when these cues are not the intended focus of our diagnostic protocol. In contrast, silhouette-based retrieval produces neighbors with more diverse visual appearances, since face, jersey, and texture are removed from the input. This difference is consistent with the observation in Secs. 6.2 and 6.3: full-appearance models can exploit static shortcuts, while appearance-suppressed models rely more on how the body is configured and moves through the free-throw routine.

G.2. Embedding-space Visualization

We further visualize the learned embedding spaces using t-SNE. Each marker denotes the cluster center of one identity, and colors indicate player identity. To compare neighborhood structure across regimes, we mark one focus identity and annotate its Top-5 nearest neighboring identity centers in the appearance and silhouette feature spaces.

As shown in Fig. G2, the nearest-neighbor structure changes substantially after appearance is suppressed. In the appearance feature space, the focus identity is surrounded by one set of neighboring identities, whereas in the silhouette feature space its closest neighbors are reorganized and reordered. This indicates that the two regimes do not simply produce the same identity geometry under different in-

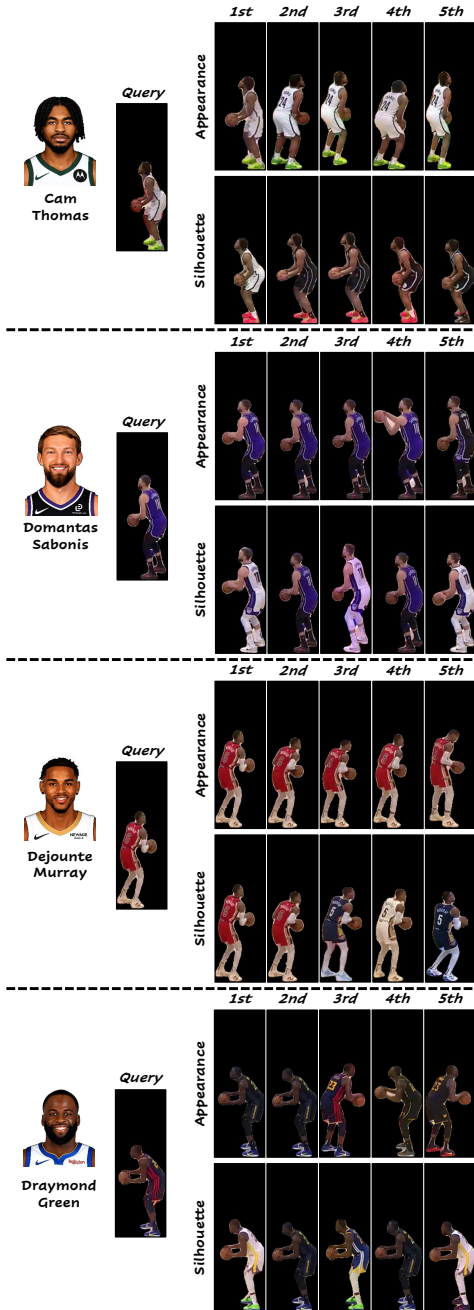


Figure G1. Top-5 nearest gallery clips retrieved under appearance and silhouette inputs. Appearance retrieval tends to preserve visual similarity, while silhouette retrieval returns appearance-diverse clips.

put channels. Instead, appearance and silhouette inputs induce different neighborhood structures, suggesting that the learned representations emphasize different cue families.

This visualization complements the retrieval examples in §G.1. Appearance-based representations tend to organize clips according to static visual similarity, while silhouette-based representations are more consistent with appearance-

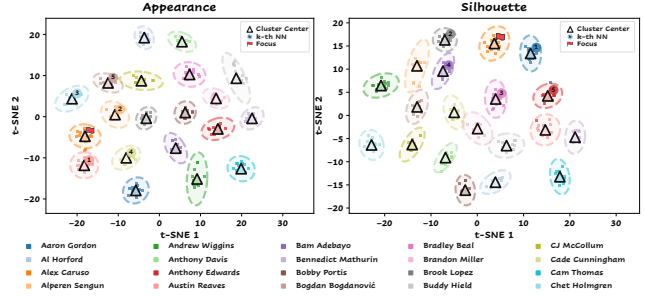


Figure G2. t-SNE visualization of identity-level cluster centers under appearance and silhouette inputs. The red flag marks the same focus identity, and numbers indicate its Top-5 nearest neighboring identity centers in each feature space. The changed neighbor ordering shows that appearance and silhouette models organize identity evidence differently.

suppressed execution evidence. We therefore treat the t-SNE discrepancy as representation-level support for the cue shift observed in Secs. 6.2 and 6.3, rather than as standalone proof of motion-based recognition.

H. Stable and Distinctive Execution Evidence

The saliency analysis in §6.3 suggests that appearance-suppressed models attend to execution-dependent evidence rather than static visual shortcuts. Here, we provide extended qualitative and quantitative support for the diagnostic criteria introduced in §B: the evidence should be stable within an identity, distinct across identities, and aligned with interpretable phases of the free-throw routine. We visualize five representative players: *Al Horford*, *Damian Lillard*, *Dennis Schroder*, *Jaden Ivey*, and *Jalen Williams*. As shown in Fig. H1, each row contains CAM-based saliency maps across multiple clips and pose-guided temporal saliency curves for the same identity.

H.1. Qualitative Stability and Distinctiveness

Across clips of the same player, the silhouette model repeatedly highlights similar regions at corresponding phases, indicating that the saliency patterns are not dominated by incidental frame-level noise. Across players, however, the highlighted regions and their temporal progression differ. This supports the view that the model does not rely on a single universal cue shared by all free-throws, but instead combines multiple execution-dependent cues into identity-specific motion signatures.

For *Al Horford*, the model consistently emphasizes lower-body and torso evidence during the load and rise phases, followed by increased attention to the shooting arm and upper-body finish near release. For *Damian Lillard*, saliency appears earlier and more strongly around the compact preparatory posture, including the lower body, torso, and set-point configuration, before shifting toward

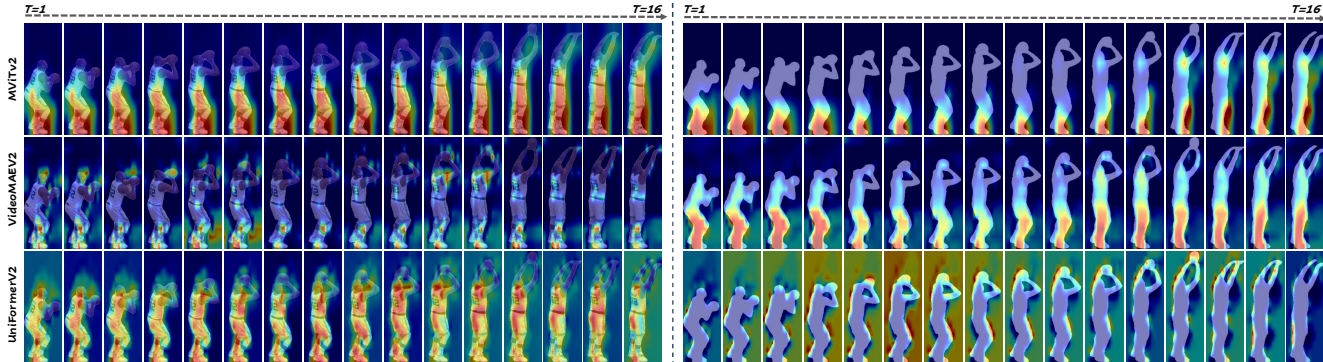


Figure 11. Backbone-dependent saliency patterns under appearance and silhouette inputs. For the same identity and sequence, MViTv2 shows a more spatially distributed response, whereas VideoMAEV2 and UniFormerV2 exhibit more localized or region-focused patterns. These qualitative differences support the view that backbones aggregate execution-dependent identity evidence at different spatial scales.

the shooting arm during release. For *Dennis Schroder*, the highlighted evidence is initially weaker and more localized, then becomes more prominent around the torso, hip, and arm trajectory as the motion progresses. For *Jaden Ivey*, the maps show a broader response over the body, consistent with a more global coordination pattern rather than a single localized joint cue. For *Jalen Williams*, the model also uses broad body evidence, but with a different temporal profile, including sustained attention to standing stability and upper-limb behavior during the later shooting phases.

These player-wise patterns indicate that identity-specific motion signatures are compositional. They are not defined by one isolated body part, such as only the arm or only the feet. Instead, the model appears to combine phase-specific posture, lower-body loading, torso alignment, limb coordination, and follow-through configuration. This interpretation is consistent with our diagnostic design in §3, where execution-dependent evidence can appear within individual phases and also unfold across transitions between phases.

H.2. Pose-guided Quantitative Saliency Curves

To quantitatively complement the frame-level saliency maps, we aggregate saliency values over pose-guided anatomical regions. Using estimated keypoints, we group the body into head, torso, arms, and legs, and compute region-level saliency over the sequence. The resulting curves in Fig. H1 provide a temporally resolved quantitative summary of how the model’s focus evolves across the free-throw routine.

These quantitative profiles reinforce the qualitative observations. First, they show phase-aligned temporal structure: saliency shifts across body regions as the action moves from set posture to rise, release, and follow-through. Second, they show identity-specific profiles: different players exhibit different saliency trajectories even though they perform the same action. Third, they are consistent with the spatial maps, indicating that the pose-guided curves sum-

marize the same evidence observed in the CAM visualizations rather than introducing an unrelated measurement.

Taken together, the qualitative saliency maps and quantitative pose-guided curves support the central claim that appearance-suppressed models recover stable, distinctive, and interpretable execution evidence. The resulting motion signature is best understood as a structured combination of body-region cues and phase-specific dynamics, rather than as a single localized visual feature. As in §B, we interpret these results as diagnostic evidence for model behavior, not as standalone proof.

I. Backbone-dependent Saliency Patterns

We finally compare saliency patterns across the three video backbones under the same identity and sequence. This analysis complements the backbone-sensitivity discussion in §C: if different architectures aggregate identity evidence at different spatial scales, their saliency maps should reveal different patterns even when the input sequence and target identity are fixed.

As shown in Fig. 11, the three backbones exhibit visibly different saliency distributions. MViTv2 produces a relatively broad and spatially distributed response, with highlighted regions spanning the lower body, torso, and upper body as the free-throw progresses. VideoMAEV2 shows a more localized pattern, especially under appearance input, where attention concentrates on smaller regions rather than covering the full body trajectory. UniFormerV2 exhibits an intermediate but more region-focused behavior, with saliency often concentrated around selected body parts or phase-specific configurations. These differences are also visible under silhouette input, where static appearance cues are removed. MViTv2 continues to aggregate evidence over a broader body region across time, whereas VideoMAEV2 and UniFormerV2 show more concentrated responses around local execution cues. This observation is

consistent with the hypothesis in §C.2: backbones that aggregate evidence more globally may be more robust when the input is reduced to sparse skeletons, while models that rely more heavily on localized regional evidence may be more sensitive to the loss of dense spatial structure.

Importantly, these patterns do not imply that one backbone uses a single cue and another uses a different single cue. Rather, they suggest that identity-specific motion signatures can be represented through different architectural strategies. The evidence remains execution-dependent, but the spatial scale at which each backbone organizes that evidence differs. We therefore treat this comparison as qualitative support for the broader claim that motion signatures are compositional and architecture-dependent, rather than tied to one fixed saliency pattern.

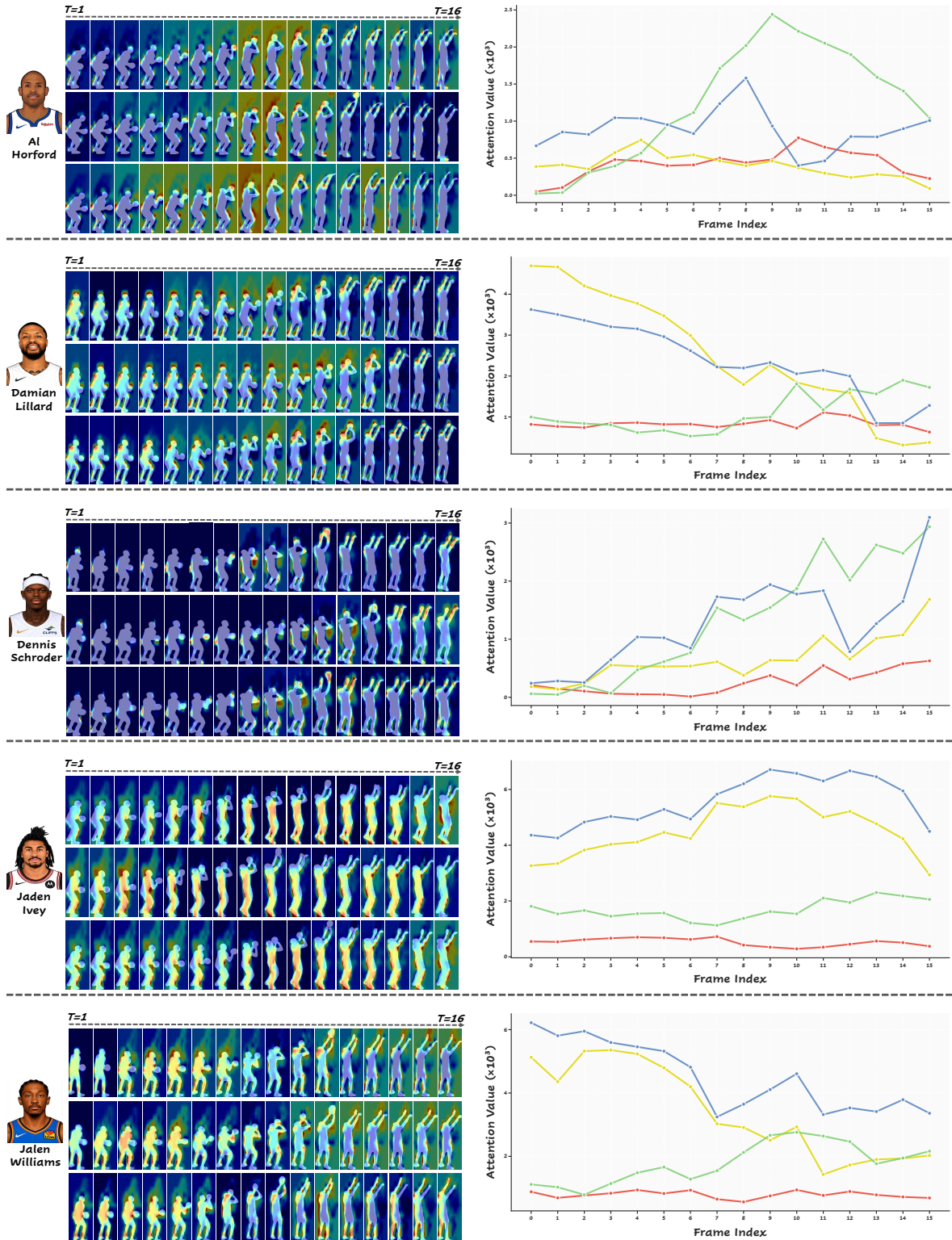


Figure H1. Stable and distinctive execution evidence across five identities. For each player, the left panel shows CAM-based saliency maps over multiple clips through the sequence, while the right panel reports pose-guided quantitative saliency curves over anatomical regions: **Head**, **Torso**, **Arms**, and **Legs**. The saliency patterns remain consistent within each identity but differ across identities, supporting the view that motion signatures emerge from compositional, phase-aligned execution cues rather than a single localized body part.